Reactive ion etching of high optical quality GaN/sapphire photonic crystal slab using CH_4-H_2 chemistry

S. Bouchoule[a)]
Laboratoire de Photonique et de Nanostructures (LPN), CNRS UPR 020, Route de Nozay, 91 460 Marcoussis, France

S. Boubanga-Tombet
Groupe d'Etude des Semiconducteurs (GES), CNRS UMR 5650, Université Montpellier II, Place Eugène Bataillon, 34 095 Montpellier Cedex 05, France

L. Le Gratiet
Laboratoire de Photonique et de Nanostructures (LPN), 91 460 Marcoussis, France

M. Le Vassor d'Yerville and J. Torres
Groupe d'Etude des Semiconducteurs (GES), 34 095 Montpellier Cedex 05, France

Y. Chen
Laboratoire de Photonique et de Nanostructures (LPN), 91 460 Marcoussis, France

D. Coquillat
Groupe d'Etude des Semiconducteurs (GES), 34 095 Montpellier Cedex 05, France

(Received 12 September 2006; accepted 30 November 2006; published online 20 February 2007)

Reactive ion etching (RIE) using a CH_4-H_2 plasma is investigated for the fabrication of a GaN one-dimensional (1D) photonic crystal (PhC) slab. The dominant control parameter for the etch rate and the sidewall profile is the dc bias. The influence of operating pressure, CH_4/H_2 ratio, and total gas flow rate on the etching characteristics is also presented. An etch rate as high as 85 nm/min and an overcut angle as low as 5° obtained in this work are among the best values reported for conventional RIE technique. The CH_4-H_2 process is used to etch 1D PhCs with a lattice parameter ranging from 700 to 350 nm and an air filling factor of 0.30 into a 600-nm-thick GaN/sapphire slab. Sharp peaks corresponding to the resonant modes of the nanopatterned structures are observed in the experimental reflection spectra for all the lattice periods. Furthermore, the good optical quality of the nanostructures is evidenced by a resonantly enhanced second-harmonic generation experiment around 400 nm. A second-harmonic generation enhancement factor as high as 10^5 is obtained, compared with the unpatterned GaN reference slab. These results demonstrate that the CH_4-H_2 conventional RIE technique is well adapted to the etching of GaN PhC for the fabrication of next generation photonic devices exploiting nonlinear processes. © *2007 American Institute of Physics*. [DOI: 10.1063/1.2433770]

I. INTRODUCTION

Nanopatterning of GaN-based devices is a promising technology for many applications in the UV to blue-green wavelength range. Research in this area in recent years has been mainly focused on the realization of two-dimensional (2D) photonic crystals (PhCs) on the top of GaN-based LEDs to improve the light extraction efficiency and to control the emission directionality. The light extraction mechanism, with PhC used as output grating couplers, is being studied both theoretically and experimentally for various lattice geometries.[1,2] Light extraction enhancement in the range of 50%–150% has been demonstrated for blue[3–6] and UV [7,8] electrically driven LEDs. The fabrication of high-Q PhC resonant nanocavities having potential interest for ultralow threshold lasers, single photon sources, or investigation of the strong coupling regime has also been reported recently in the 460–500 nm wavelength range.[9] Finally, nanopatterning of the GaN membrane slab with one-dimensional (1D) and 2D PhC has also proven very efficient to enhance nonlinear optical processes such as second- and third-harmonic generation from the infrared (IR) to blue and UV wavelength range.[10–12]

From the processing point of view, the nanopatterning of GaN-based epitaxial layers poses a number of challenges, and techniques to increase control and obtain low-damage etching are still being developed. Due to the short wavelength range being considered, the fabrication of GaN-based PhCs requires high precision lithography and etching techniques. Spatial disorder as well as etched surface roughness leading to unwanted light scattering can be a critical issue. Moreover, due to the wide band gap and high bond strength (e.g., 8.9 eV/atom for GaN) of group-III nitride materials, the dry etching techniques generally used rely on a very important physical component to assist the chemical etch and to promote both bond breaking and sputter desorption of III- and N–reaction products. This may in turn degrade the structural quality of the material, leading to optical and carrier nonradiative losses. Finally, the strong physical component

[a)]Electronic mail: sophie.bouchoule@lpn.cnrs.fr

 © 2007 American Institute of Physics

Downloaded 21 Feb 2007 to 193.48.163.6. Redistribution subject to AIP license or copyright, see http://jap.aip.org/jap/copyright.jsp

of etching generally leads to a positively sloped sidewall (i.e., overcut profiles), related to the conventional effect of tilt angle on sputter yield. Overcut angles (i.e., deviation from perfect verticality) generally lie in the range from 20° to 10° whatever reactive ion etching technique used.[3,9] The asymmetry induced in the PhC pattern can cause a deviation of the PhC behavior from the ideal theoretical prediction. Furthermore, the overcut angle can limit the maximal etching depth, which will be a critical issue for the etching of PhC with a low air filling factor (<0.3) into a relatively thick (>500 nm) GaN slab. Dry etching processes with a lower surface roughness, lower damage, reduced overcut angle, and reasonable etching rate are thus required for this purpose.

Dry processing of GaN and related materials has been extensively investigated in previous years using different etching systems and various reactive gas mixtures. Ion beam techniques such as reactive ion beam etching[13] (RIBE) or chemically assisted Ar ion beam etching[14–16] (CAIBE) have been used with Cl_2 and BCl_3 as reactive gases. Typically, etch rates in the range of 50–200 nm/min have been obtained, with CAIBE obtaining highly vertical profiles (~0° overcut angle) by using a high sample temperature[14] or by optimizing the Ar beam incidence angle.[15,16] However, reactive ion etching (RIE) techniques have been the most widely studied, including conventional RIE, electron cyclotron resonance (ECR) RIE, and inductively coupled plasma (ICP) RIE. For conventional RIE, smooth etching and GaN etch rates between 20 and 100 nm/min have been reported.[17–27] Theses results were mostly obtained with chlorinated plasma chemistries, including $SiCl_4$-(Refs. 17–19) and BCl_3-(Refs. 20 and 21) based gas mixtures. The halogen gas HBr has also been investigated.[22] Generally fluorinated plasmas including SF_6,[23] C_2ClF_5, and CHF_3[24] reactive gases have led to lower etch rates (<30 nm/min), larger overcut angle, and potentially a poor selectivity with dielectric mask. The addition of a small amount of SF_6 to $SiCl_4$[23,25] or BCl_3[26] was shown to increase the etch rate by a factor of ~4, typically up to 200 nm/min, and to smooth the etched surface. However, recent experimental studies using $SF_6/SiCl_4/Ar$ RIE indicated that the overcut angle is likely to increase with the addition of SF_6.[27] In all cases, sloped sidewalls were generally reported with typical overcut angles from 30° to 10°.

ECR and ICP RIE techniques systematically led to higher GaN etching rates, in the range from 100 nm/min to several hundreds of nm/min, due to their higher ion density. The most commonly used plasma chemistry is based on Cl_2 and BCl_3 reactive gases or their combination, diluted with Ar or N_2, and with H_2 eventually added to the mixture.[28–32] Highly anisotropic profiles have been obtained using ICP RIE,[32,37–40] but a deviation from perfect sidewall verticality by 10° -20° is still often observed with these techniques.[28,33–36] The highly anisotropic ICP processes generally rely on a relatively high dc bias around 300–400 V.[32,39,40]

The effect of adding CH_4 to the above mentioned gas mixtures has been investigated in both ICP[29,34] and ECR[28,30,33,41] RIEs. CH_4 allows the formation of III-CH_x reaction products which are more volatile than their III-chloride counterparts.[42] $CH_4/Cl_2/Ar$ was thus shown to be particularly suitable for smooth ICP etching of GaN/InGaN heterostructures.[34] H_2 is generally added to CH_4 since the N element can be expelled as NH_x while it is expelled as NCl_x or perhaps free N_2 in Cl_2-based mixtures. Again the volatility of NH_3 compares favorably with that of NCl_3.[42] Consequently, $CH_4/H_2/Ar$[30,33,41] and $CH_4/H_2/Cl_2/Ar$[28,29] chemistries were investigated in ECR-RIE. No detailed information was presented on the sidewall profile, but an overcut angle of approximately 12° can be deduced from the SEM images of Ref. 28.

Only a few experimental studies have been devoted to CH_4-based conventional reactive ion etching of GaN and related materials. Smooth etched surfaces and GaN etch rates from 50 to 80 nm/min have been reported using $CH_4/H_2/Ar$[41] and $Cl_2/CH_4/H_2/Ar$[29] gas mixtures, with no detailed information provided on the sidewall angle. Coquillat *et al.*[43] investigated a pure CH_4/H_2 RIE technique to etch GaN pillars and demonstrated that relatively smooth surfaces and overcut angles as low as 9° could be obtained with a typical etch rate of 50 nm/min. This chemistry could therefore be adapted to the nanopatterning of GaN slabs.

In this paper we report a detailed investigation of reactive ion etching of GaN/sapphire membrane slabs with CH_4-H_2 chemistry. The dc bias is shown to be the main parameter in achieving high etch rates with overcut angles smaller than 10°. The influence of working pressure, CH_4-H_2 ratio, and total gas flow rate on the etch rate, overcut angle, and carbonated polymers redeposition is also presented. Conditions are found for which an etching rate of 85 nm/min and an overcut angle of 5° together with a smooth etched surface are obtained. The CH_4-H_2 process is used to etch 1D PhC patterns with lattice periods ranging from 700 to 350 nm into a 600-nm-thick GaN/sapphire membrane slab. The high optical quality of the patterned structures is assessed by an enhanced blue second-harmonic generation (SHG) experiment, in which the second harmonic signal is generated by coupling an IR pump signal to a resonant photonic mode.

II. PROCESS OPTIMIZATION

The samples consist of a 600–800 nm-thick nonintentionally doped GaN epilayer grown by metal organic chemical vapor deposition on 2 in. sapphire substrates, with the *c* axis of the GaN crystal normal to the surface. The choice of the GaN layer thickness is the result of wanting to maintain a moderately high multimode GaN waveguide slab for our photonics applications, while at the same time avoiding poor structural quality of the epilayer. Obtaining thin high-quality GaN epilayers on sapphire substrates is very difficult, and surface pitting is present on the surface of the as-grown layers that would be transferred during the etching process. However, we observed that the pit density after etching was similar to that of the as-grown samples. Hence the pits cannot be taken as an indication of the etching process performance.

The RIE reactor chamber is made of aluminum. The 100 mm diameter stainless steel cathode, with a silicon cover plate on top of it, is driven by a 0–300 W 13.56 MHz rf

Downloaded 21 Feb 2007 to 193.48.163.6. Redistribution subject to AIP license or copyright, see http://jap.aip.org/jap/copyright.jsp

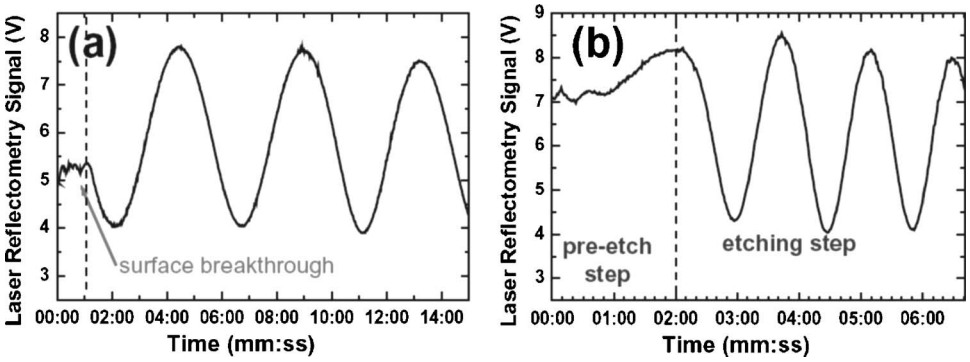

FIG. 1. (a) A typical laser reflectometry curve of a sample etched with 200 W rf power, 40 mT pressure, 65 sccm total gas flow rate, and $CH_4/H_2=0.25$. (b) A laser reflectometry curve of a typical etching sequence. The parameters for the etching step (second step) are 270 W rf power, 100 mT pressure, 116 sccm total gas flow rate, and $CH_4/H_2=0.45$. The plasma is ignited at $t=00:00$.

generator. The cathode temperature is set to 20 °C by water cooling. The reactor is equipped with CH_4, H_2, and O_2 gas lines, and a laser reflectometry system is integrated in the equipment for real-time monitoring of the etch depth.

Wafers were patterned with a mask of 500 μm long periodic rectangular stripes having a width varying in a staircase shape from 10 to 2 μm. This pattern was used in order to be able to estimate in a reproducible way the overcut angle at the mesa edge without fracturing the samples. We used a hybrid metal-dielectric mask consisting of 100 nm Ni deposited on a 300-nm-thick plasma-enhanced chemical vapor deposition (PECVD) SiN_x layer using the lift-off technique, with subsequent anisotropic etching of the SiN_x layer in SF_6/CHF_3 RIE using Ni as a mask. Ni was used because of its high resistance to sputtering and its low etch rate in CH_4/H_2 RIE, so that the influence of mask erosion and shape transfer effect on the etched GaN sidewall profile was minimized. In all the following etching experiments, we found that the 100 nm Ni layer was never completely etched whatever the process parameters investigated. The wafers were cut into 10×10 mm^2 samples for the study.

The GaN etch rate was estimated using stylus profilometry, after the mask was removed in diluted HF. The carbonated polymer redeposition rate on top of the mask was also estimated by comparing the mesa height measured on as-etched samples, and then measured after a RIE O_2 ashing process to remove the carbonated polymers from the Ni surface. Surface roughness and sidewall profile were inspected by scanning electron microscopy (SEM). The overcut angle was systematically measured by inspection of the mesa edge using SEM at 88° incidence from normal with the stripes oriented in the direction of the observation, in order to obtain reproducible and comparable results.

The effects of rf power, working pressure, CH_4/H_2 ratio, and total gas flow rate were investigated for process optimization. The etch depth was fixed to 450 nm and was monitored by the laser reflectometry signal. The etch time was consequently varied, depending on the process parameter values.

A typical laser reflectometry curve is shown in Fig. 1(a). A delay in the onset of GaN etching is clearly observed at the beginning of the process. This could be related to the presence of an oxidized layer on the GaN surface. Auger electron spectroscopy[44] and x-ray photoelectron spectroscopy[45,46] studies have shown that both O and C are largely incorporated in the GaN surface, and that a gallium oxide/oxynitride layer can readily form when oxygen is present, particularly in the case of Ga-rich surface or with dangling Ga bonds. This oxidized layer can be critical in CH_4-H_2 plasma, since this chemistry is prone to carbonated polymer redeposition on all inert surfaces. A competition between carbon redeposition and etching can occur at the beginning of the plasma process, and we observed that the GaN etching can even be blocked for certain parameter values if the oxidized surface is not removed. In order to avoid the surface breakthrough delay that may lead to incorrect and nonreproducible etch rates, all etching experiments were carried out with a pre-etch step having a fixed duration of 2 min. The other parameters of the pre-etch step were 40 mT working pressure, 65 sccm total gas flow rate, $CH_4/H_2=0.25$, and 200 W rf power. A reproducible surface breakthrough was achieved under such conditions and was found to be relatively independent of the GaN surface state, with an etch depth of 20 nm. The laser reflectometry curve of a typical etching process sequence is illustrated in Fig. 1(b).

A. Influence of rf power

It is expected from previous studies on GaN etching that the main control for the etch rate is exerted by the dc bias. The etch rate is reported in Fig. 2(a) as a function of rf power for 40 mT working pressure, 65 sccm total flow rate, and $CH_4/H_2=0.25$. The variation of the dc bias with rf power is reported in Fig. 2(b). A rf power of 100 W (dc bias= −600 V) is required to achieve an etch rate value of 10 nm/min, and a quasilinear increase of the etch rate is observed in the 100–200 W power range. The carbonated polymer redeposition rate measured on top of the mask is also reported in Fig. 2(a). It does not significantly change with rf power between 100 and 200 W. As can be seen, the GaN etch rate and redeposition rate become very similar for an rf power less than 70 W. We believe that a competition between etching and redeposition may occur at the GaN surface at that point, leading to somewhat nonreproducible results. The overcut angle is reported as a function of rf power in Fig. 2(b) and is found to decrease with the rf power. Highly anisotropic profiles with a measured overcut angle values less than 8° were obtained at a rf power of 200 W (dc bias of −940 V). A SEM image of the mesa edge profile under these conditions is given in the inset of Fig. 2(a). The dc bias was thus fixed at a high value of −940 V in the following etching experiments.

Downloaded 21 Feb 2007 to 193.48.163.6. Redistribution subject to AIP license or copyright, see http://jap.aip.org/jap/copyright.jsp

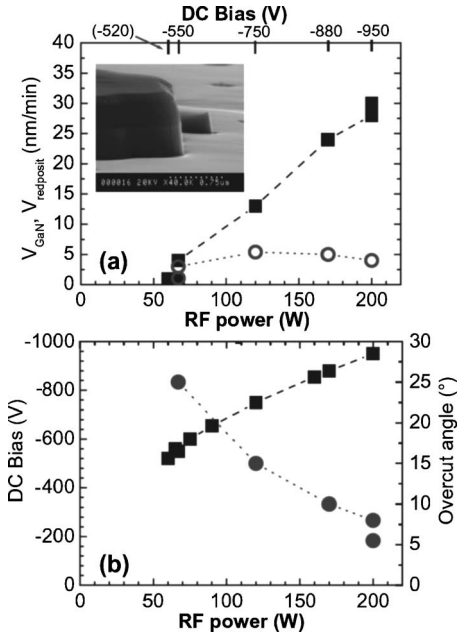

FIG. 2. (a) The GaN etch rate (squares) and polymer redeposition rate (open circles) as a function of rf power (Inset: SEM image of GaN etched with 200 W rf power. The mask is still present, and polymers are not removed). (b) dc bias (squares, left axis) and overcut angle (circles, right axis) as a function of rf power.

B. Effect of working pressure

The variation of the GaN etch rate as a function of working pressure is presented in Fig. 3. The CH_4/H_2 ratio was fixed to 0.25. The rf power was adjusted to maintain a constant dc bias of −940 V during the etching step, and the corresponding values are reported as a function of pressure in the figure. Changing both pressure and rf power obviously modifies the plasma dissociation and thus the chemical part of the etching, but this effect cannot be decoupled from ion energy in conventional RIE, and following the results of Fig. 2 we assumed that the dc bias has the dominant influence on the etching rate. Carbonated polymer redeposition can also affect the GaN etching process, and the redeposition rate may increase for larger gas residence time, as experimentally evidenced in CH_4–H_2 plasma studies for the etching of InP.[47] When changing the pressure, we adjusted the total flow rate in order to maintain a constant gas residence time, or at least fixed the flow rate to its highest value achievable with our gas inlet and pumping system. The flow rate value is indicated for each pressure on the top axis in Fig. 3. The corresponding gas residence times are nearly constant and are 0.76, 0.70, 0.85, 0.91, and 0.99 s for 20, 40, 60, 80, and 100 mT, respectively.

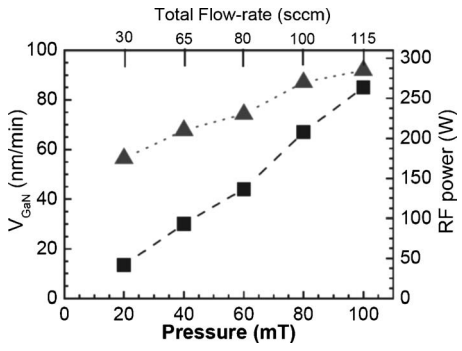

FIG. 3. The GaN etch rate (squares, left axis) and rf power required to maintain a constant dc bias of −940 V (triangles, right axis) as a function of pressure. The total flow rate values set for the different pressure values are indicated on the top axis.

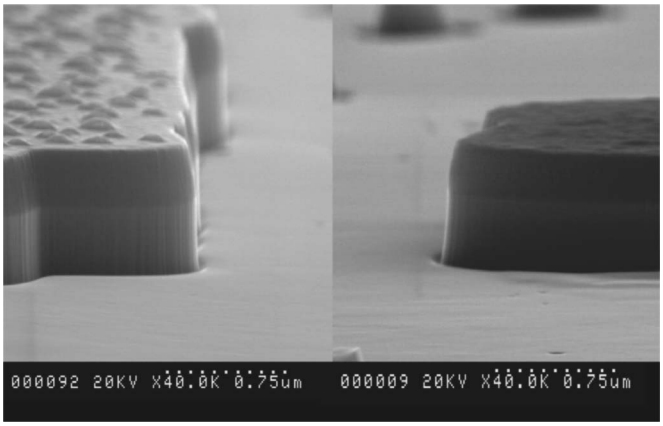

FIG. 4. A SEM image of GaN mesa etched with a SiN_x/Ni mask for a working pressure of 80 mT (left) and 100 mT (right). Ni is still present in both cases and polymers are not removed.

Under these conditions, the polymer redeposition rate measured on top of the mask showed no significant variation with pressure and was in the range of 3–4.5 nm/min within the experimental measurement error. On the other hand, the GaN etch rate increased, and a value of 85 nm/min is obtained for 100 mT, which is among the highest values reported for RIE. Highly anisotropic profiles were obtained in the 40–100 mT pressure range with a measured overcut angle less than 8°. Overcut angles as low as 5°–6° were systematically measured in the 80–100 mT pressure range. However, microtrenching at the bottom of the mesa edge was observed for 80 and 100 mT, as illustrated in Fig. 4.

C. Effect of CH_4/H_2 ratio

The effect of the CH_4/H_2 ratio on the GaN etch rate is reported in Fig. 5. The polymer redeposition rate is also reported in this figure. Other parameters were a 100 mT working pressure, −940 V dc bias, and 100 sccm total gas flow rate. The GaN etch rate increased with the CH_4/H_2 ratio up to a ratio of ~0.25, and then saturated to remain at a value ~85 nm/min. On the other hand, the polymer redeposition

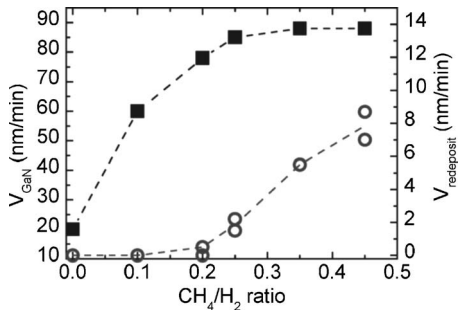

FIG. 5. The GaN etch rate (squares, left axis) and polymer redeposition rate (open circles, right axis) as a function of CH_4/H_2 ratio, with other parameters fixed to P=100 mT, total flow rate=100 sccm, and dc bias=−940 V.

Downloaded 21 Feb 2007 to 193.48.163.6. Redistribution subject to AIP license or copyright, see http://jap.aip.org/jap/copyright.jsp

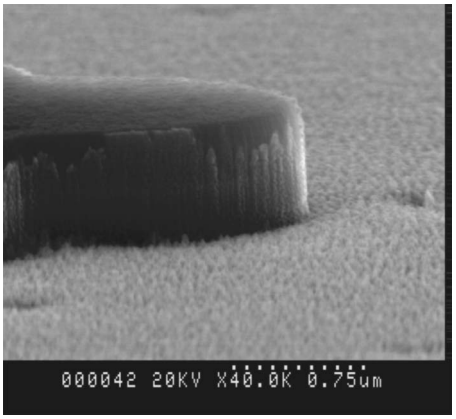

FIG. 6. SEM image of a GaN sample etched with 0% methane concentration.

rate increased constantly with increased methane concentration. Therefore, a ratio of 0.25 appeared to be a good compromise for an optimized etching process. For ratio's lower than 0.25, the GaN etch rate became significantly lower, but it was still approximately 20 nm/min for pure hydrogen plasma. This is an indication of the strong physical component and sputtering effect under high dc bias. However, the surface was extremely rough and grassy in that case, as illustrated in Fig. 6, and redeposition of some nonvolatile products could be observed on the mesa edge, this latter effect still being present for up to 20% methane concentration. Chemical removal of the Ga element as a volatile metal organic compound is thus necessary to obtain smooth etched surface and sidewalls.

We finally investigated the influence of total flow rate on the etching performance, with the other parameters set to $CH_4/H_2=0.25$, dc bias=−940 V, and pressure=40 mT. Starting with a flow rate of 65 sccm, corresponding to the highest achievable value with our pumping system, we found that the GaN etch rate decreased by a factor of ~6 (from 30 to 6 nm/min) when the flow rate was decreased by a factor of 5. A competition between etching and carbonated polymer formation and redeposition could explain this behavior. For a fixed working pressure, the flow rate should therefore be set to its highest achievable value. Finally, in an attempt to reduce the redeposition rate, we added a small amount of oxygen to the gas mixture. A decrease in the redeposition rate was observed, but the GaN etch rate was drastically reduced at the same time: for 40 mT pressure, −940 V dc bias, 65 sccm total flow rate, and $CH_4/H_2=0.25$, the etch rate was reduced by a factor of ~6, from 30 to 4.7 nm/min when 0.7 sccm of O_2 was added to the gas mixture. This effect is probably due to the oxyde layer forming on the GaN surface and competing with the etching process. This is consistent with recent spectroscopic studies of GaN and AlGaN surfaces exposed to O_2 containing plasmas.[48,49]

III. PROCESSING OF 1D PHOTONIC CRYSTAL SLAB

The CH_4-H_2 process was used to etch one-dimensional PhC in a 600-nm-thick GaN slab to perform nonlinear SHG experiments. A 300-nm-thick SiN_x layer was first deposited on the GaN/sapphire slab by PECVD. The PhC patterns were defined by e-beam lithography, evaporation of 50 nm Ni, and subsequent lift-off. They were then transferred using dry etching into the SiN_x layer in the same manner as for the previous samples, defining 360×360 μm^2 PhC areas. The PhCs were designed to present a fixed air filling factor of 0.30, and periods of 700, 500, 450, 400, and 350 nm. Bulk areas of GaN covered with Ni/SiN_x were also defined near the PhC regions and were used as bulk GaN reference in the nonlinear optical characterizations.

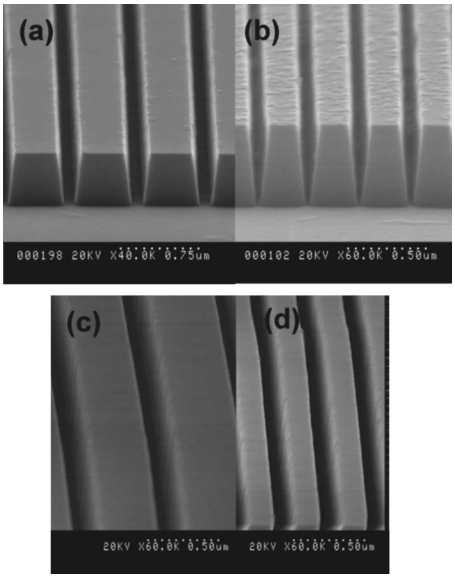

FIG. 7. SEM images of the GaN etched PhCs with 700 nm [(a) and (c)] and 350 nm [(b) and (d)] period. Defects apparent on the nanopatterns in (a) and (b) are due to the sputtering step of gold cap layer. They disappeared after chemical removal of gold [(c) and (d)].

GaN was etched using CH_4-H_2 conventional RIE with 60 mT pressure, −940 V dc bias, 80 sccm total gas flow rate, and $CH_4/H_2=0.25$. The sample was then cleaned for 10 min in an oxygen plasma and the mask was removed in diluted HF. SEM images of the 700 and 350 nm period PhCs are reported in Figs. 7(a)–7(d). The sample was capped with 20 nm sputtered gold for observation to avoid charging effects from the insulating sapphire surface. Despite the reduction of the Ni layer thickness to 50 nm, we still observed smooth etching with no degradation of the etched profile, as seen in Fig. 7. The small overcut angle of 6° measured from the SEM images allowed to etch completely the 600-nm-thick GaN slab down to the sapphire substrate even for the 350 nm period.

IV. LINEAR AND NONLINEAR OPTICAL CHARACTERIZATIONS

The experimental setup used to perform linear and nonlinear characterizations of the 1D PhC has been presented in detail in previous work.[10,12] For the linear characterization, a broadband collimated light source was used, while for the SHG experiments, a femtosecond titanium:sapphire laser beam focused on the sample to a spot size of ~30 μm was used as a source. In the following, and to be consistent with previous descriptions,[10,12] φ denotes the azimuthal angle. It corresponds to the angle between the Γ-X symmetry direc-

Downloaded 21 Feb 2007 to 193.48.163.6. Redistribution subject to AIP license or copyright, see http://jap.aip.org/jap/copyright.jsp

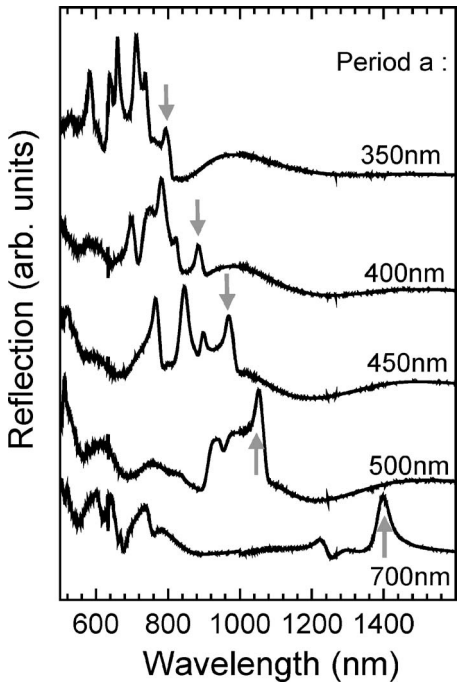

FIG. 8. Reflection spectra measured along the Γ-*X* symmetry direction ($\varphi=0°$) for an angle of incidence of $\theta=5°$ and for *p*-polarized incident light, for the PhCs with period $a=700$, 500, 450, 400, and 350 nm. An arrow indicates the first-order photonic mode for each period.

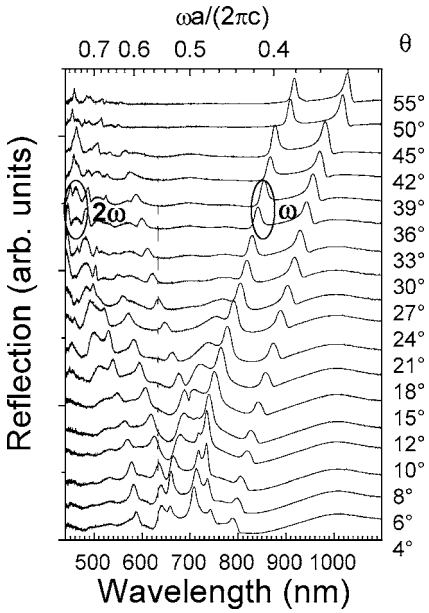

FIG. 9. Reflection spectra measured as a function of the angle of incidence θ for the 350 nm period PhC, along the Γ-*X* symmetry direction ($\varphi=0°$).

tion of the 1D PhC (i.e., normal to the GaN stripes) and the plane of incidence perpendicular to the GaN surface and including the incident laser beam. The angle θ denotes the incidence angle and corresponds to the angle formed by the incident beam and the normal to the GaN surface.

Figure 8 shows the reflection spectra measured along the Γ-*X* symmetry direction ($\varphi=0°$) for *p*-polarized incident light with θ fixed at 5°, for the 700, 500, 450, 400, and 350 nm period PhCs. The sharp resonant features superimposed on a slowly oscillating background are due to the coupling of the light with *p* modes of the photonic band structure. With decreasing PhC period *a*, features due to the mode coupling are observed to shift to lower wavelength, as expected since their positions scale approximately as *a*. The higher-wavelength mode of each PhC indicated by arrows in Fig. 8 corresponds to the first-order photonic mode.

The θ-dependent reflection spectra of the 350 nm period PhC measured along the Γ-*X* direction are shown in Fig. 9. The angle of incidence θ was varied from 0° to 58°. When θ is increased, the peaks corresponding to the coupling of the incident beam to the resonant modes of the PhC are clearly observed to disperse. For an incident angle θ between 36° and 39°, both modes at frequency ω and at frequency 2ω become resonant modes of the PhC, as indicated by the circles in Fig. 9. The experimental photonic band diagram along the Γ-*X* symmetry direction, corresponding to the plot of the frequency position of the resonances as a function of the incident light in-plane wave-vector amplitude, is reported in Fig. 10 for *p*-polarized incident light. Along the Γ-*X* symmetry direction, all photonic modes are pure *p* modes since no polarization conversion occurs. The dashed construction line in the figure corresponds to a fixed angle of incidence θ of 38.5°. The circles at ω ($\lambda=848$ nm) and 2ω ($\lambda/2=424$ nm) at $\theta=38.5°$ denote the condition where quasi-phase-matching occurs with simultaneous confinement of the fundamental mode (ω) and the second-harmonic mode (2ω). The SHG exaltation factor defined as the intensity of the second-harmonic signal generated from the 1D PhC normalized against the intensity of the second-harmonic signal generated from the unpatterned reference GaN slab, was measured under this resonant-resonant configuration. We measured an exaltation factor of 1.10^5, corresponding to an improvement by more than one order of magnitude compared to the best value of 7500[11] previously obtained using the same experimental setup from a 1D PhC GaN slab etched

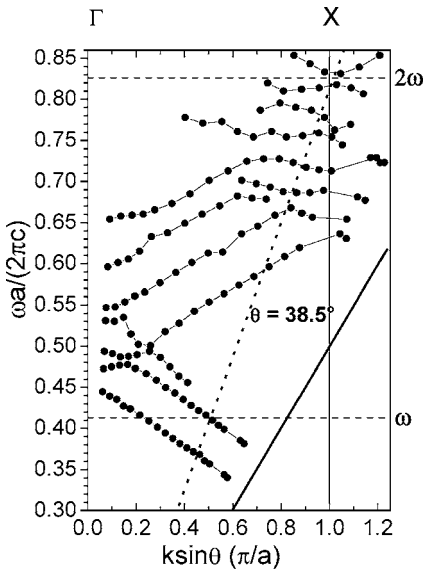

FIG. 10. Experimental photonic band structure along the Γ-*X* symmetry direction for *p*-polarized incident light. The dark solid line shows the accessible light cone with external coupling techniques. The dashed construction line corresponds to a fixed θ of 38.5°.

Downloaded 21 Feb 2007 to 193.48.163.6. Redistribution subject to AIP license or copyright, see http://jap.aip.org/jap/copyright.jsp

using $SiCl_4$ RIE. Moreover, a SHG intensity of 1.25 μW could be directly be measured under these optimized conditions.

V. CONCLUSION

We used the CH_4-H_2 conventional RIE technique for the etching of GaN nanopatterns and thoroughly investigated the effects of dc bias, working pressure, and CH_4/H_2 ratio on the etching performance. An etch rate as high as 85 nm/min and an overcut angle smaller than 8° together with a smooth etched surface were obtained under optimized conditions. The process was used to etch 1D PhC patterns into a 600-nm-thick GaN/sapphire membrane slab. The high optical quality of the patterned structures was assessed by resonantly enhanced blue SHG experiments, and a SHG enhancement factor of 10^5 was obtained compared with an unpatterned GaN reference slab. This is significantly higher than the enhancement factors of 5000–7500 [10,11] and of ~250[12] previously reported for 1D and 2D GaN PhC slabs, respectively, and demonstrates that conventional CH_4-H_2 RIE is a simple processing technique well suited to 1D or 2D nanopatterning of GaN for next generation photonic devices.

ACKNOWLEDGMENTS

The authors would like to gratefully acknowledge Olivier Briot and Sandra Ruffenach, from Groupe d'Etude des Semiconducteurs CNRS-Université Montpellier 2, for the growth of the GaN epitaxial layers. Part of this work was supported by the European Network of Excellence PHOREMOST. Dr. C. S. Corr from Plasma Research Laboratory, ANU, Canberra, Australia is acknowledged for his critical reading of the manuscript.

[1] A. David *et al.*, Appl. Phys. Lett. **87**, 101107 (2005).
[2] A. David, T. Fujii, E. Matioli, R. Sharma, S. Nakamura, S. P. DenBaars, C. Weisbuch, and H. Benisty, Appl. Phys. Lett. **88**, 073510 (2006).
[3] J. J. Wierer, M. R. Krames, J. E. Epler, N. F. Gardner, M. G. Craford, J. R. Wendt, J. A. Simmons, and M. M. Sigalas, Appl. Phys. Lett. **84**, 3885 (2004).
[4] D.-H. Kim *et al.*, Appl. Phys. Lett. **87**, 203508 (2005).
[5] T. Kim, A. J. Danner, and K. D. Choquette, Electron. Lett. **41**, 1138 (2005).
[6] Z. S. Zhang, B. Zhang, J. Xu, K. Xu, Z. J. Yang, Z. X. Qin, T. J. Yu, and D. P. Yu, Appl. Phys. Lett. **88**, 171103 (2006).
[7] T. N. Oder, K. H. Kim, J. Y. Lin, and H. X. Jiang, Appl. Phys. Lett. **84**, 466 (2004).
[8] J. Shakya, K. H. Kim, J. Y. Lin, and H. X. Jiang, Appl. Phys. Lett. **85**, 142 (2004).
[9] Y.-S. Choi *et al.*, Appl. Phys. Lett. **87**, 243101 (2005).
[10] J. Torres *et al.*, Phys. Rev. B **691**, 085105 (2004).
[11] J. Torres, M. le Vassor d'Yerville, D. Coquillat, E. Centeno, and J. P. Albert, Phys. Rev. B **71**, 195326 (2005).
[12] D. Coquillat, G. Vecchi, C. Comashi, A. M. Malvezzi, J. Torres, and M. Le Vassor d'Yerville, Appl. Phys. Lett. **87**, 101106 (2005).
[13] J. Lee, H. Cho, D. C. Hays, C. R. Abernathy, S. J. Pearton, R. H. Shul, G. A. Vawter, and J. Han, IEEE J. Sel. Top. Quantum Electron. **4**, 557 (1998).
[14] A. T. Ping, I. Adesida, and M. A. Khan, Appl. Phys. Lett. **67**, 1250 (1995).
[15] M. Kneissl, D. P. Bour, N. M. Johnson, L. T. Romano, B. S. Krusor, R. Donaldson, J. Walker, and C. Dunnrowicz, Appl. Phys. Lett. **72**, 1539 (1998).
[16] F. Binet, J.-Y. Duboz, N. Laurent, C. Bonnat, P. Collot, F. Hanauer, O. Briot, and R. L. Aulombard, Appl. Phys. Lett. **72**, 960 (1998).
[17] I. Adesida, A. Mahajan, E. Andideh, M. Asif Khan, D. T. Olsen, and J. N. Kuznia, Appl. Phys. Lett. **63**, 2777 (1993).
[18] D. Peyrade, Y. Chen, L. Manin-Ferlazzo, A. Lebib, N. Grandjean, D. Coquillat, R. Legros, and J. P. Lascaray, Microelectron. Eng. **57**, 843 (2001).
[19] T. Talierco *et al.*, Superlattices Microstruct. **36**, 783 (2004).
[20] M. E. Lin, Z. F. Fan, Z. Ma, L. H. Allen, and H. Morkoç, Appl. Phys. Lett. **64**, 887 (1994).
[21] Q. Fan, S. Chevtchenko, X. Ni, S.-J. Cho, F. Yun, and H. Morkoç, J. Vac. Sci. Technol. B **24**, 1197 (2006).
[22] A. T. Ping, I. Adesida, M. Asif Khan, and J. N. Kuznia, Electron. Lett. **30**, 1895 (1994).
[23] F. Karouta, B. Jacobs, P. Vreugdewater, N. G. H. van Melick, O. Schoen, H. Protzman, and M. Heuken, Electrochem. Solid-State Lett. **2**, 240 (1999).
[24] H. Lee, D. B. Oberman, and J. S. Harris, Appl. Phys. Lett. **67**, 1754 (1995).
[25] F. Karouta, B. Jacobs, O. Schoen, and M. Heuken, Phys. Status Solidi A **176**, 755 (1999).
[26] M. S. Feng, J. D. Guo, Y. M. Lu, and E. Y. Chang, Mater. Chem. Phys. **45**, 80 (1996).
[27] E. Sillero, F. Calle, and M. A. Sanchez-Carcia, J. Mater. Sci.: Mater. Electron. **16**, 409 (2005).
[28] R. J. Shul, S. P. Kilcoyne, M. Hagerott Crawford, J. E. Parmeter, C. B. Vartuli, C. R. Abernathy, and S. J. Pearton, Appl. Phys. Lett. **66**, 1761 (1995).
[29] R. J. Shul, G. B. McClellan, S. J. Pearton, C. R. Abernathy, C. Constantine, and C. Barrat, Electron. Lett. **32**, 1408 (1996).
[30] S. J. Pearton, C. R. Abernathy, and F. Ren, Appl. Phys. Lett. **64**, 2294 (1994).
[31] T. Wu, Z.-B. Hao, G. Tang, and Y. Luo, Jpn. J. Appl. Phys., Part 2 **42**, L257 (2003).
[32] R. J. Shul *et al.*, Appl. Phys. Lett. **69**, 1119 (1996).
[33] T. Arakawa *et al.*, Jpn. J. Appl. Phys., Part 1 **44**, 5819 (2005).
[34] H. K. Kim, H. Lin, and Y. Ra, J. Vac. Sci. Technol. A **22**, 598 (2004).
[35] K. Zhu, V. Kuryatkov, B. Borisov, G. Kipshidze, S. A. Nikishin, H. Temkin, and M. Holtz, Appl. Phys. Lett. **81**, 4688 (2002).
[36] Y. B. Hahn, Y. H. Im, J. S. Park, K. S. Nahm, and Y. S. Lee, J. Vac. Sci. Technol. A **19**, 1277 (2001).
[37] R. J. Shul, G. Vawter, C. G. Willison, M. M. Bridges, J. W. Lee, S. J. Pearton, and C. R. Abernathy, Solid-State Electron. **42**, 2259 (1998).
[38] C. Youtsey and A. Adesisa, *Handbook of Advanced Plasma Processing Techniques*, edited by R. J. Shul and S. J. Pearton (Springer, Berlin, 2000), Chap. 11, p. 489.
[39] E. Zhirnov, S. Stepanov, A. Gott, W. N. Wang, Y. G. Shreter, D. V. Tarkhin, and N. I. Bockhareva, J. Vac. Sci. Technol. A **23**, 687 (2005).
[40] D. S. Y. Hsu, C. S. Kim, C. R. Eddy, R. T. Holm, R. L. Henry, J. A. Casey, V. A. Shamanian, and A. Rosenberg, J. Vac. Sci. Technol. B **23**, 1611 (2005).
[41] C. B. Vartuli, J. D. MacKenzie, J. W. Lee, C. R. Abernathy, S. J. Pearton, and R. J. Shul, J. Appl. Phys. **80**, 3705 (1996).
[42] *CRC Handbook of Chemistry and Physics*, 85th ed., edited by D. R. Lide (CRC, Boca Raton, FL, 2004).
[43] D. Coquillat, S. K. Murad, A. Ribayrol, C. J. M. Smith, R. M. De La Rue, C. D. W. Wilkinson, O. Briot, and R. L. Aulombard, Mater. Sci. Forum **264–268**, 1403 (1998).
[44] S. Y. Han, H. S. Hang, K. H. Baik, S. J. Pearton, and F. Ren, Jpn. J. Appl. Phys., Part 1 **44**, 7234 (2005).
[45] S. Tripathy, A. Raman, S. J. Chua, and A. Huan, J. Vac. Sci. Technol. A **19**, 2522 (2001).
[46] Y.-J. Han, S. Xue, W.-P. Guo, C.-Z. Sun, Z.-B. Hao, and Y. Luo, Jpn. J. Appl. Phys., Part 1 **42**, 6409 (2003).
[47] T. R. Hayes, M. A. Dreisbach, P. M. Thomas, W. C. Dautremont-Smith, and L. A. Heimbrook, J. Vac. Sci. Technol. B **7**, 1130 (1989).
[48] J.-M. Lee, K.-M. Chang, I.-H. Lee, and S.-J. Park, J. Vac. Sci. Technol. B **18**, 1409 (2000).
[49] Y. Han, S. Xue, W. Guo, Y. Luo, Z. Hao, and C. Sun, Jpn. J. Appl. Phys., Part 2 **42**, L1139 (2003).

Downloaded 21 Feb 2007 to 193.48.163.6. Redistribution subject to AIP license or copyright, see http://jap.aip.org/jap/copyright.jsp